357.1) Ices in planet-forming disks: Self-consistent ice opacities in disk models
Aditya M. Arabhavi, Peter Woitke, Stephanie M. Cazaux, Inga Kamp, Christian Rab, Wing-Fai Thi

357.2) Tracing the contraction of the pre-stellar core L1544 with HC17O+ J = 1-0 emission
J. Ferrer Asensio, S. Spezzano, P. Caselli, F. O. Alves, O. Sipilä, E. Redaelli, L. Bizzocchi, F. Lique, A. Mullins

357.3) Volatile-rich comets ejected early on during Solar System formation
S.E. Anderson, J.-M. Petit, B. Noyelles, O. Mousis, P. Rousselot

357.4) The Star Formation-Gas Density Relation in Four Galactic GMCs: Effects of Stellar Feedback
John H. Bieging, Shuo Kong

357.5) Possible Explosive Dispersal Outflow in IRAS 16076-5134 revealed with ALMA
Estrella Guzmán Ccolque, Manuel Fernández-López, Luis A. Zapata, Tapas Baug

357.6) Turbulence and Accretion: a High-resolution Study of the B5 Filaments
Michael Chun-Yuan Chen, James Di Francesco, Jaime E. Pineda, Stella S. Offner, Rachel K. Friesen

357.7) Rethinking the role of the giant planet instability in terrestrial planet formation models
Matthew S. Clement, Rogerio Deienno, Andre Izidoro

357.8) Turbulence in outer protoplanetary disks: MRI or VSI?
Can Cui, Xue-Ning Bai

357.9) A Population of Dipper Stars from the Transiting Exoplanet Survey Satellite Mission
Benjamin K. Capistrant, Melinda Soares-Furtado, Andrew Vanderburg, Marina Kounkel, Saul A. Rappaport, Mark Omohundro, Brian P. Powell, Robert Gagliano, Thomas Jacobs, Veselin B. Kostov, Martti H. Kristiansen, Daryll M. LaCourse, Allan R. Schmitt, Hans Martin Schwengeler, Ivan A. Terentev

357.8) Turbulence in outer protoplanetary disks: MRI or VSI?

Can Cui, Xue-Ning Bai

the magnetorotational instability (MRI) and the vertical shear instability (VSI)どちらが優勢か？
ambipolar Elsaasser numbers (Am)

Am=0.1 VSI>MRI
Am=10 VSI<MRI

★MRI r>30AUでは、AD（非理想MHD効果）により弱まる。乱流に効かないだろう
★VSI （Goldreich–Schubert–Fricke不安定性）円筒状回転からのずれ

両方入れた計算はない。

Disk Model

$$\rho \propto r^{-q_D} \quad q_D = -2 \quad H = c_s/\Omega_K$$
$$T \propto r^{-q_T} \quad q_T = -1$$

$$\tau \equiv \tau_{cool}/P_{orb}$$ 無次元冷却時間

$$\Delta T = (T_{eq} - T)\left[1 - \exp\left(-\frac{\Delta t}{t_{cool}}\right)\right]$$

瞬間冷却

両極性拡散効く

効かない

最内側の回転周期

Table 1. List of simulation models and parameters.

Model	β_0	Am	τ	Runtime (P_0)
Am0.1c	10^4	0.1	0	3000
Am1c	10^4	1	0	3000
Am10Ec	10^4	10	0	3000
Am0.1	10^4	0.1	1	3000
Am1	10^4	1	1	3000
Am10E	10^4	10	1	3000

$$Am \equiv v_A^2/(\eta_A \Omega_K)$$ 両極性拡散のエルサッサー数=回転時間/イオン中性運動量交換時間

瞬時
冷却

$\tau = 1$

円周方向に平均したvz

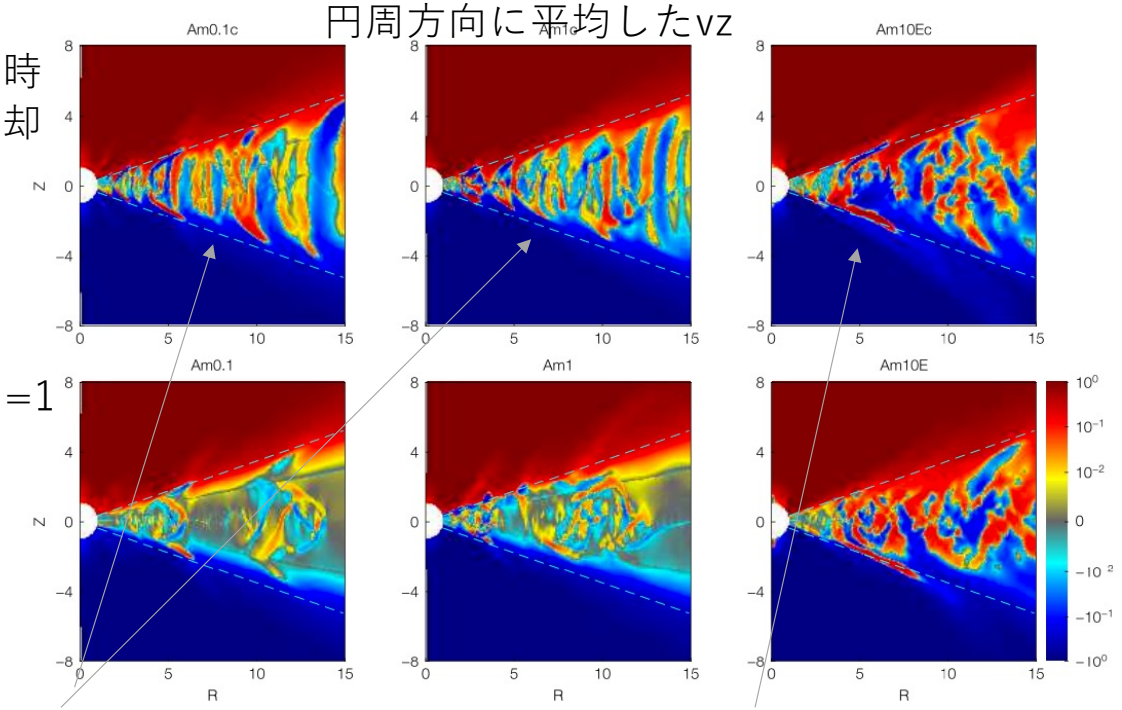

Vertical Shear Inst

Magneto Rotational Inst

$$\mathrm{ACF}(\Delta \ln R) = \frac{\langle V_z(R) V_z(R+\Delta R)\rangle}{\langle V_z^2\rangle}.$$

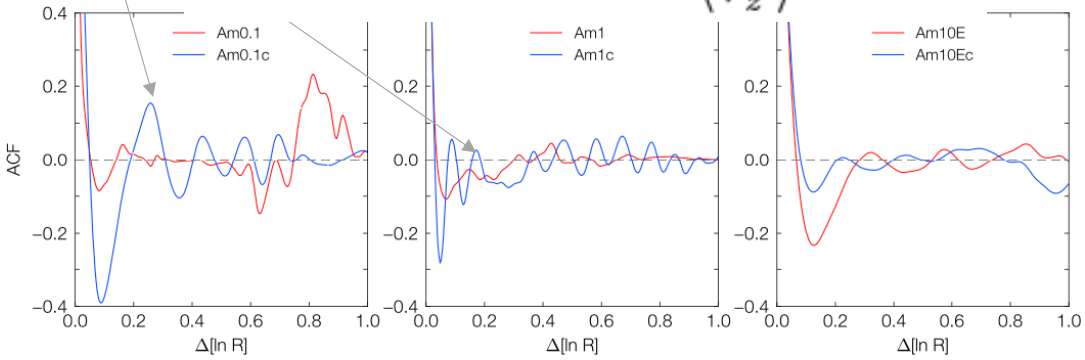

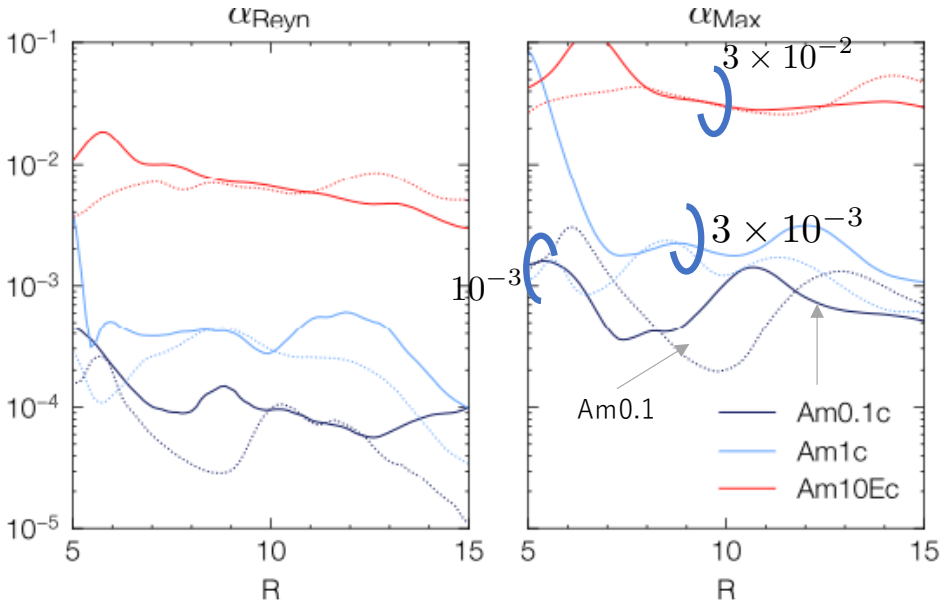

$R < B_\theta >_\phi$

ϕ 平均のポロイダル磁束

ϕ とz方向に平均したBz/Bz(t=0)

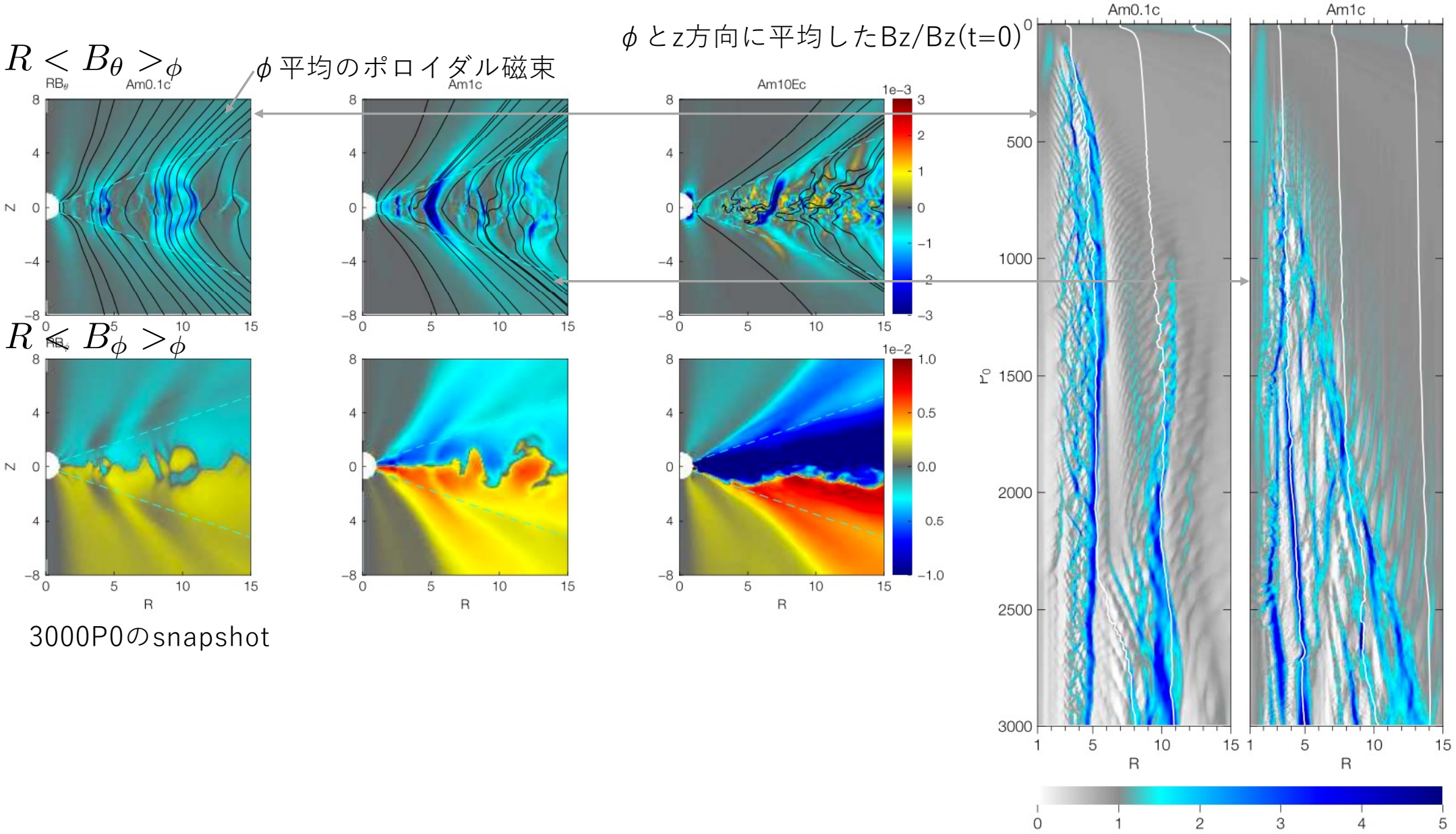

$R < B_\phi >_\phi$

3000P0のsnapshot

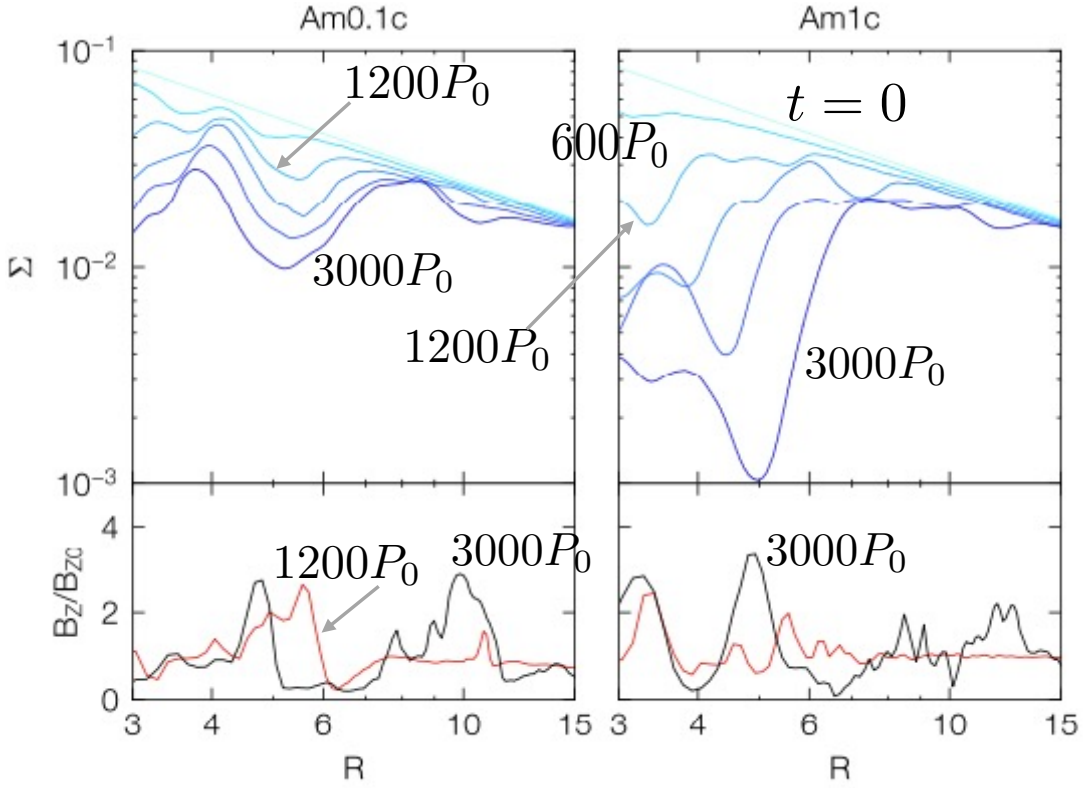
Am0.1c
Am1c
10^{-1}
10^{-2}
10^{-3}
Σ
$1200P_0$
$3000P_0$
$1200P_0$
$600P_0$
$t = 0$
$3000P_0$
$1200P_0$
$3000P_0$
$3000P_0$
B_Z/B_{Z0}
4
2
0
3
4
6
10
15
R

CB21

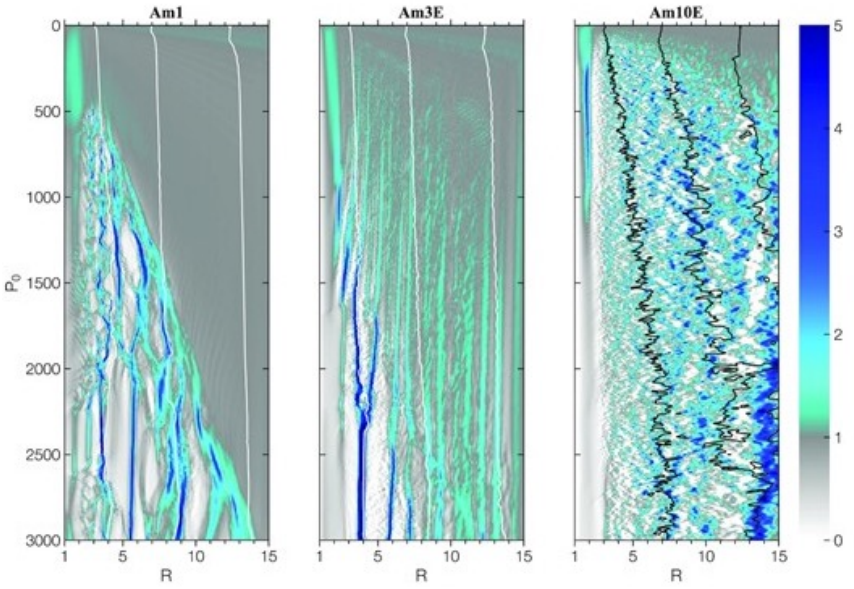
Am1
Am3E
Am10E
P_0
0
500
1000
1500
2000
2500
3000
1
5
10
15
R
5
4
3
2
1
0

357.5) Possible Explosive Dispersal Outflow in IRAS 16076-5134 revealed with ALMA

Estrella Guzmán Ccolque, Manuel Fernández-López, Luis A. Zapata, Tapas Baug

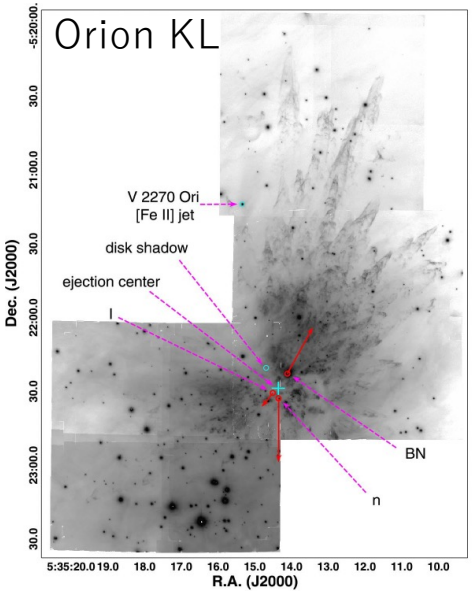

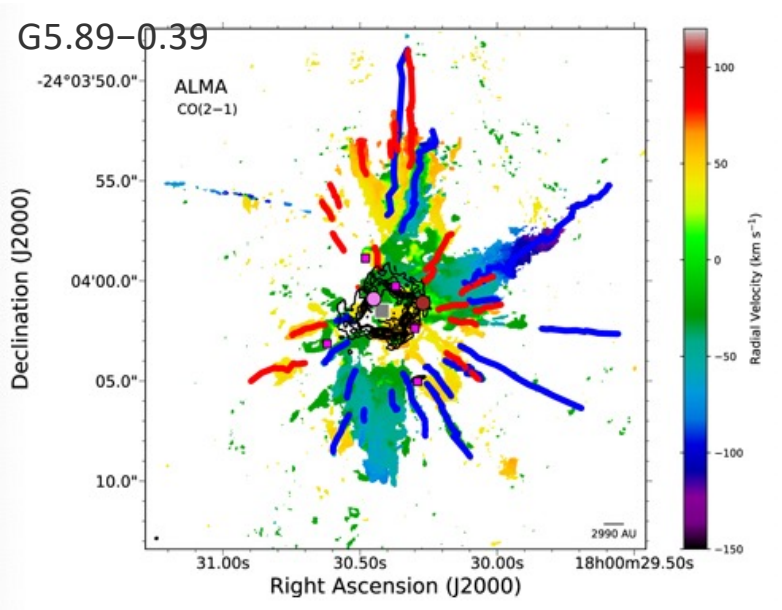

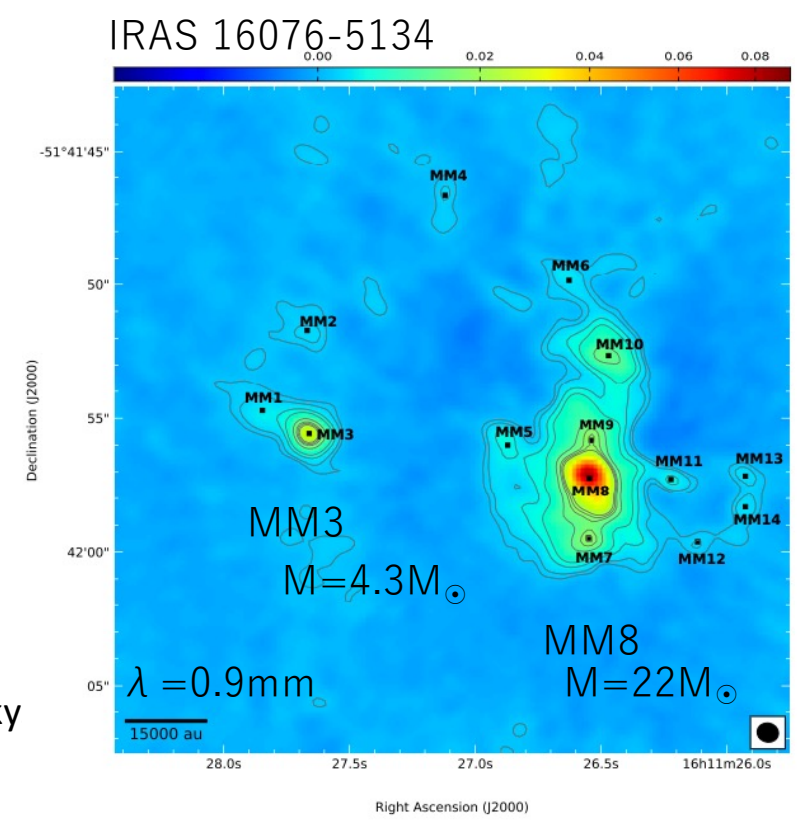

explosive dispersal outflows: new subclass of molecular outflows

dozens of filament-shaped ejections isotropically distributed on the sky
Each filament follows a well- defined Hubble velocity law

★CO, H2, [FeII]

★Narrow straight filament-like structures: isotropic, common position, Hubble's law

★The redshifted and blueshifted filaments seem to overlap in the plane of the sky.

★associated with regions of high- mass star formation

★energies are in the range of 1047 – 1049 erg.

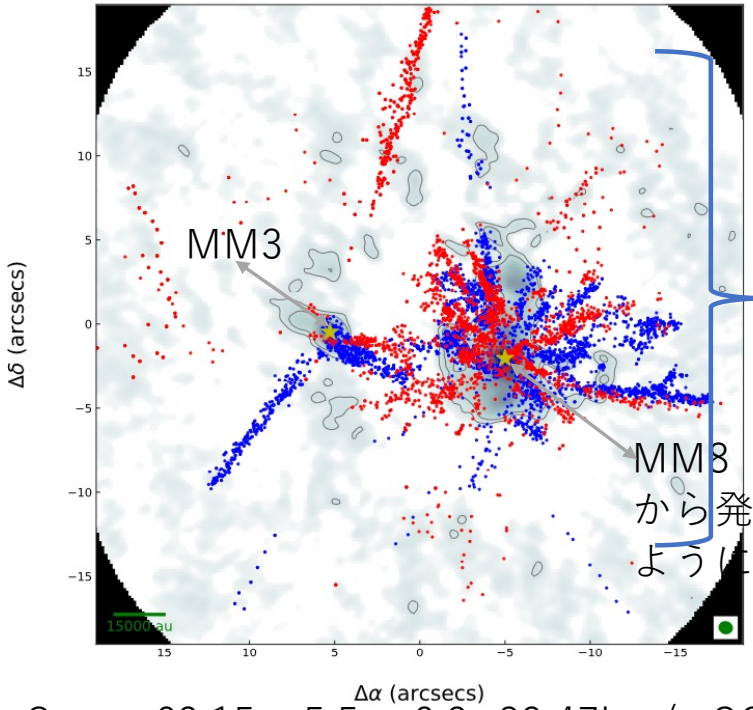

24本

赤と青12本ずつ

MM8
から発している
ように見える

quasi-isotropic distribution

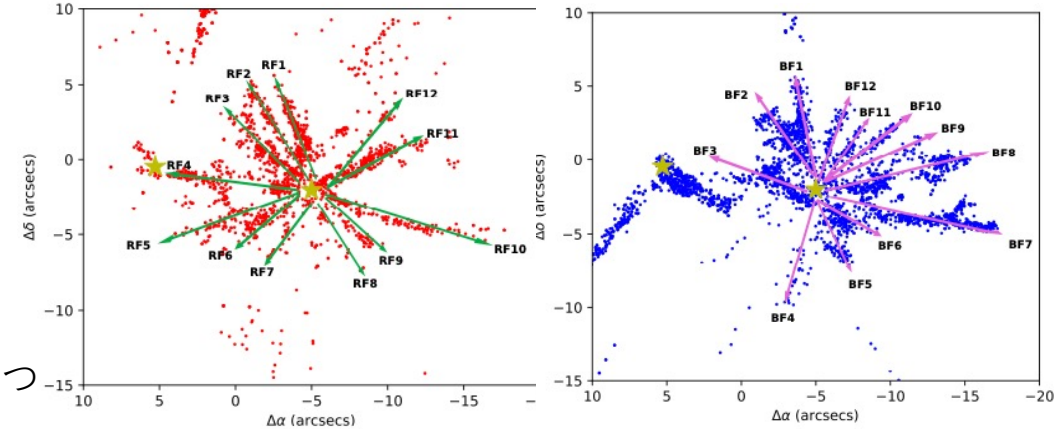

a common origin in space and velocity.

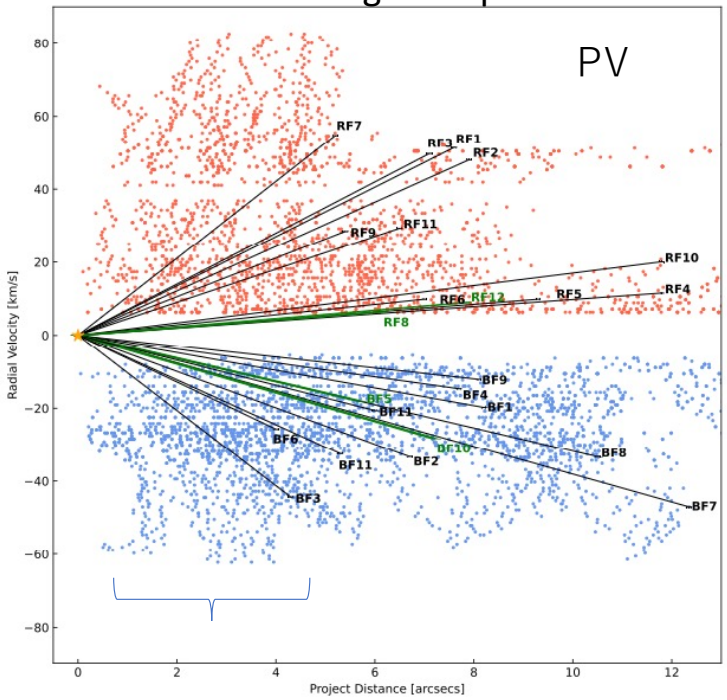

Grey: -62.15~-5.5, +6.2~83.47km/s CO(3-2) 積分強度

赤、青：Miriad cgcurs taskで探したoutflow filaments

The emission from filaments with gas at higher velocities appears more compact

Head –Tail plasmon model (Raga+ 2020)

$$u_0(\tau) = v_0 \left[1 - \left(\frac{\tau}{\tau_0}\right)^2\right] \; ; \; \text{for } |\tau| < \tau_0 \, ,$$

$$u_0(\tau) = 0 \text{ for } |\tau| \geq \tau_0$$

$$\dot{m} = \dot{M}_p/(2\pi r_j^2 \tau_0) = 2.0 \times 10^{-13} \text{ g cm}^{-2} \text{ s}^{-1} \, ,$$

$$\rho_0(\tau) = \frac{\dot{m}}{\max\left[u_0(\tau), v_{min}\right]} \, ,$$

観測された
フィラメント
状構造は
一定のVoutflow
と
天球への射影
で
よく説明される

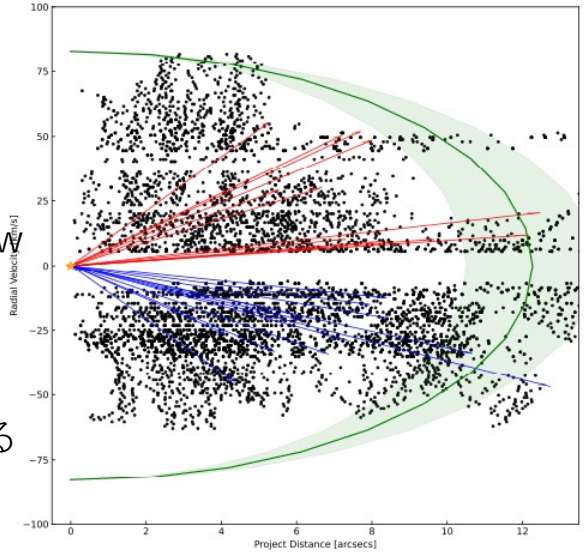

ρ_0, u_0

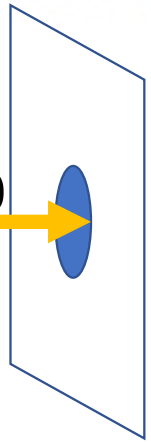

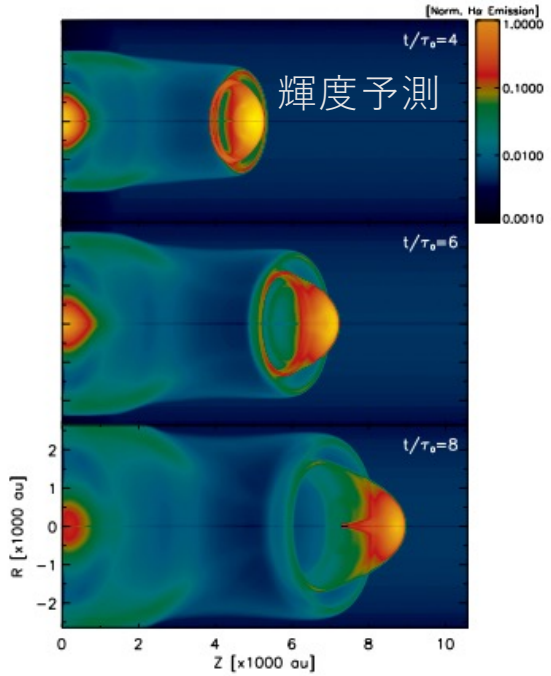

V

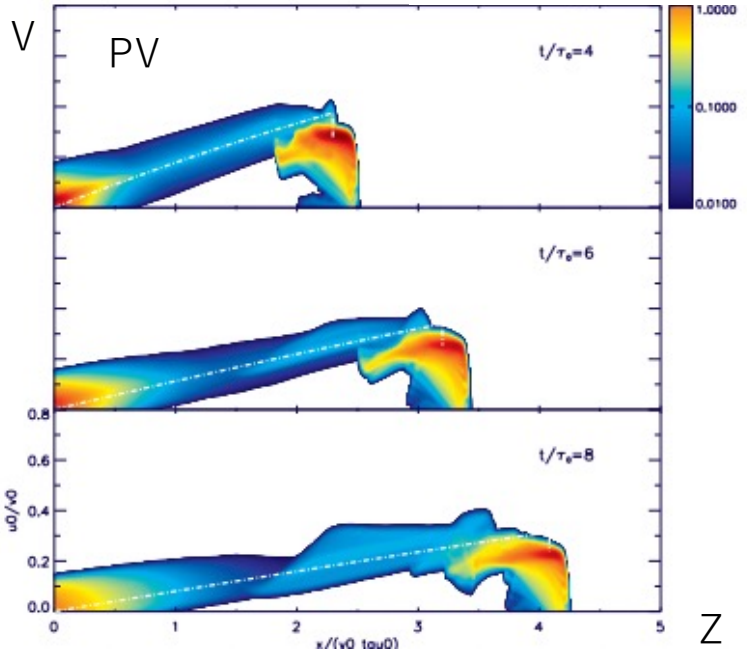

Z

357.2) Tracing the contraction of the pre-stellar core L1544 with HC17O+ J = 1-0 emission

J. F. Asensio, S. Spezzano, P. Caselli, F. O. Alves, O. Sipilä, E. Redaelli, L. Bizzocchi, F. Lique, A

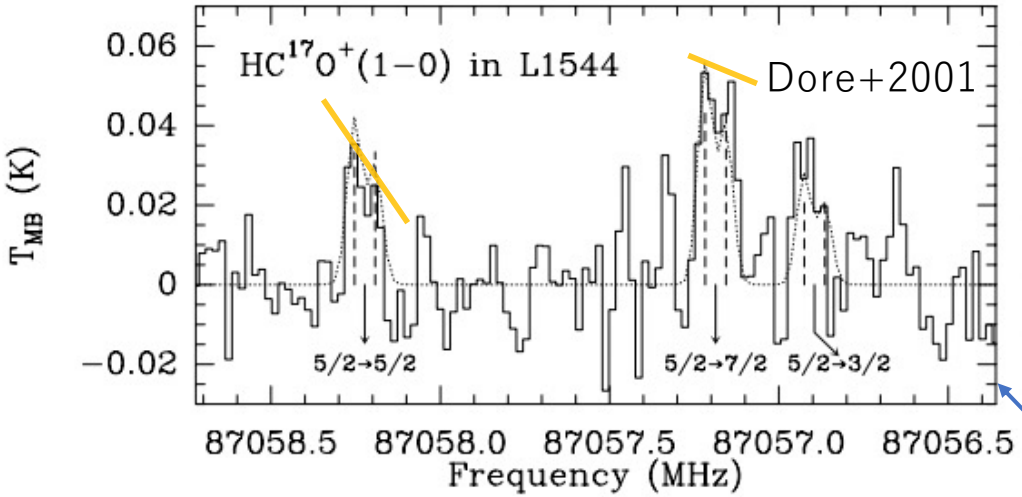

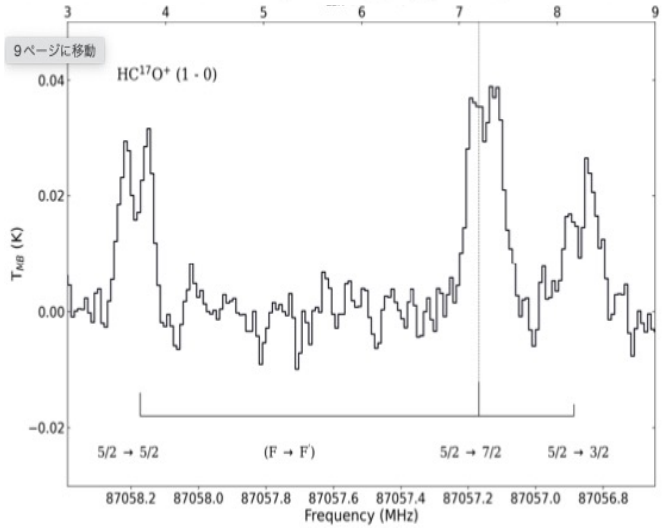

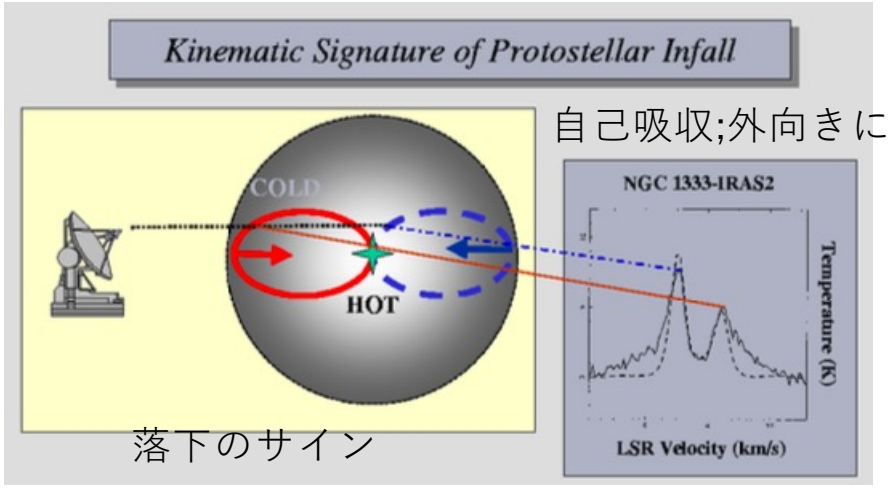

自己吸収;外向きにTex↓

落下のサイン

光学的に厚くないHC17O+(1-0)でどうして
Blue-skewed スペクトルが形成されるか

F=I+J　　I=5/2

$F \rightarrow F'$	Frequency (MHz)	E_{up} (K)	Relative intensity
5/2→3/2	87056.966(20)	4.18	2
5/2→7/2	87057.258(20)	4.18	4
5/2→5/2	87058.294(20)	4.18	3

prestellar coreのプロファイル

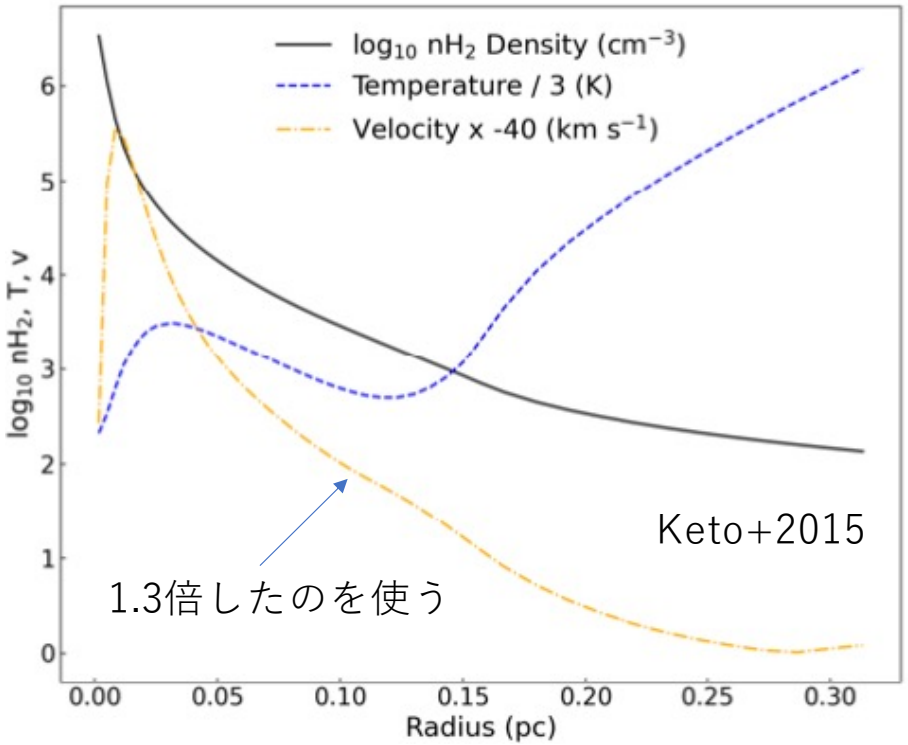

化学進化が予測するC17OとHC17O+のアバンダンス

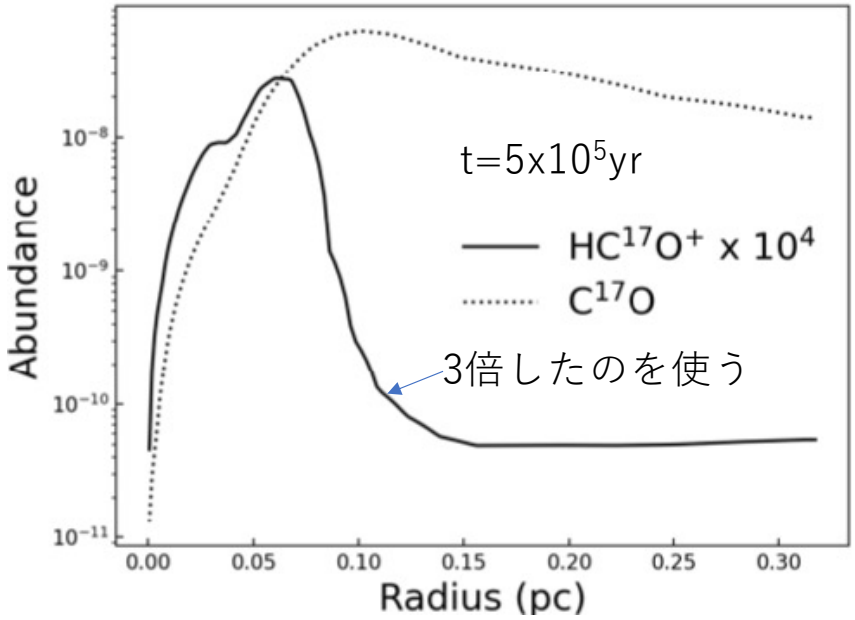

落下速度元のもの　　落下速度30%増しのもの　　Tex

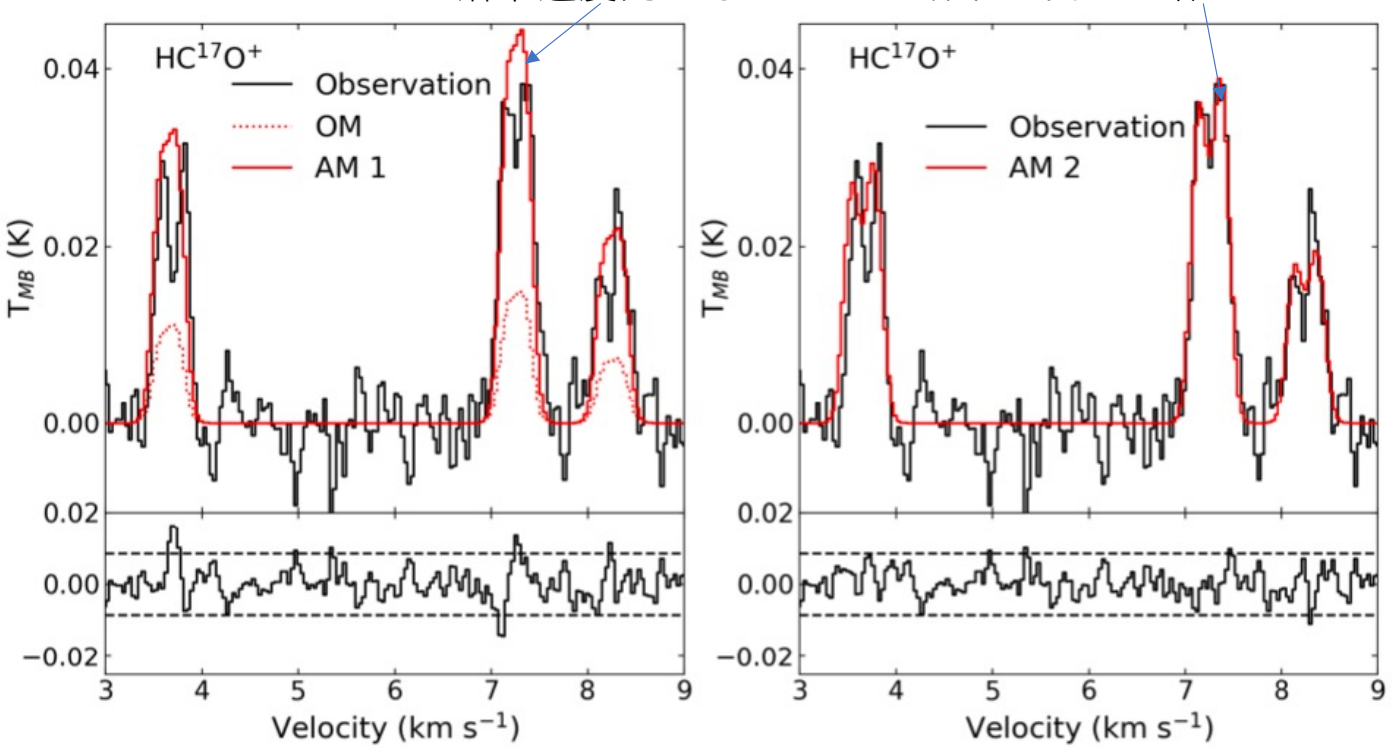

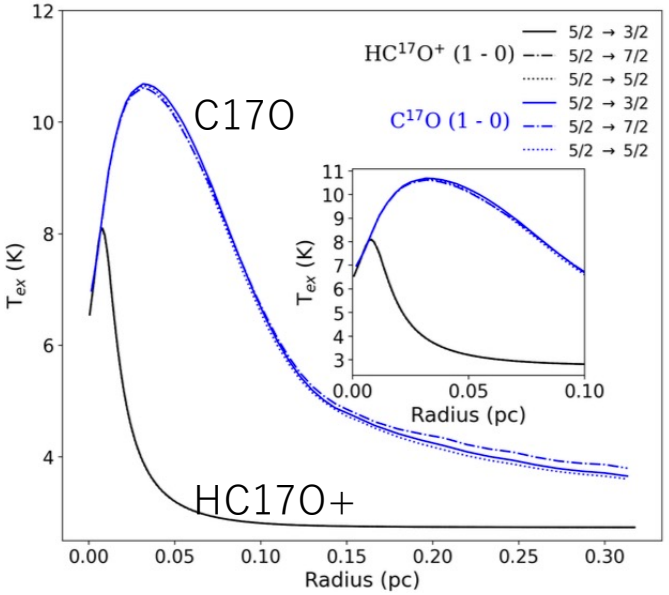

★the contraction motions at densities close to the critical density of the transition (~10^5 cm^{-3})

★the HCO+ fractional abundance decreases toward the centre

357.1) Ices in planet-forming disks: Self-consistent ice opacities in disk models

Aditya M. Arabhavi, Peter Woitke, Stephanie M. Cazaux, Inga Kamp, Christian Rab, Wing-Fai

Context. In cold and shielded environments, molecules freeze out on dust grain surfaces to form ices such as H_2O, CO, CO_2, CH_4, CH_3OH, and NH_3. In protoplanetary disks, such conditions are present in the midplane regions beyond the snowline, but the exact radial and vertical extension depend on disk mass, geometry, and stellar ultra-violet irradiation.
Aims. The goal of this work is to present a computationally efficient method to compute ice and bare-grain opacities in protoplanetary disk models consistently with the chemistry and to investigate the effect of ice opacities on the physico-chemical state and optical appearance of the disk.
Methods. A matrix of Mie efficiencies is pre-calculated for different ice species and thicknesses, from which the position dependent opacities of icy grains are then interpolated. This is implemented in the PRODIMO code by a self-consistent solution of ice opacities and the local composition of ices, which are obtained from our chemical network.
Results. Locally, the opacity can change significantly, for example, an increase by a factor of more than 200 in the midplane, especially at ultra-violet and optical wavelengths, due to ice formation. This is mainly due to changes in the size distribution of dust grains resulting from ice formation. However, since the opacity only changes in the optically thick regions of the disk, the thermal disk structure does not change significantly. For the same reason, the spectral energy distributions (SEDs) computed with our disk models with ice opacities generally show only faint ice emission features at far-IR wavelengths. The ice absorption features are only seen in the edge-on orientation. The assumption made on how the ice is distributed across the grain size distribution (ice power law) influences the far-infrared and millimeter slope of the SED. The ice features and their strengths are influenced by the ice power law and the type of chemistry. Our models predict stronger ice features for observations that can spatially resolve the disk, particularly in absorption.

357.3) Volatile-rich comets ejected early on during Solar System formation

S.E. Anderson, J.-M. Petit, B. Noyelles, O. Mousis, P. Rousselot

Context. Comet C/2016 R2 PanSTARRS (hereafter C/2016 R2) presents an unusually high N_2/CO abundance ratio, as well as a heavy depletion in H_2O, making it the only known comet of its kind. Understanding its dynamical history is therefore of essential importance as it would allow us to gain a clearer understanding of the evolution of planetesimal formation in our Solar System. Two studies have independently estimated the possible origin of this comet from building blocks formed in a peculiar region of the protoplanetary disk, near the ice line of CO and N_2.

Aims. We intend to investigate the fates of objects formed from the building blocks in these regions. We hope to find a possible explanation for the lack of C/2016 R2-like comets in our Solar System.

Methods. Using a numerical simulation of the early stages of Solar System formation, we track the dynamics of these objects in the Jumping Neptune scenario based on five different initial conditions for the protosolar disk. We integrate the positions of 250 000 planetesimals over time in order to analyze the evolution of their orbits and create a statistical profile of their expected permanent orbit.

Results. We find that objects formed in the region of the CO- and N_2- ice lines are highly likely to be sent towards the Oort Cloud or possibly ejected from the Solar System altogether on a relatively short timescale. In all our simulations, over 90% of clones formed in this region evolved into a hyperbolic trajectory, and between 1% and 10% were potentially captured by the Oort Cloud. The handful of comets that remained were either on long-period, highly eccentric orbits like C/2016 R2, or absorbed into the Edgeworth–Kuiper belt.

Conclusions. Comets formed <15 au were predominantly ejected early in the formation timeline. As this is the formation zone likely to produce comets of this composition, this process could explain the lack of similar comets observed in the Solar System.

357.4) The Star Formation-Gas Density Relation in Four Galactic GMCs: Effects of S

John H. Bieging, Shuo Kong

We present maps of 4 galactic giant molecular clouds (GMCs) in the J=2-1 emission of both CO and ^{13}CO. We use an LTE analysis to derive maps of the CO excitation temperature and column density and the distribution of total molecular gas column density, Σ_{gas}. The depletion of CO by freeze-out onto cold dust grains is accounted for by an approximation to the results of Lewis et al. (2021) which were derived from far-IR observations with *Herschel*. The surface density of young stellar objects (YSOs) is obtained from published catalogs. The mean YSO surface density exhibits a power-law dependence on Σ_{gas}, with exponents in the range 0.9 to 1.9. Gas column density probability distribution functions (PDFs) show power-law tails extending to high column densities. The distributions of sonic Mach number, M_S are sharply peaked at $M_S \sim 5-8$ for 3 GMCs; a fourth has a broad distribution up to $M_S = 30$, possibly a result of feedback effects from multiple OB stars. An analysis following the methodology of Pokhrel et al. (2021) finds that our sample of GMCs shows power-law relations that are somewhat shallower than found by Pokhrel et al. (2021) for the star formation rate vs. $\langle\Sigma_{gas}\rangle$ and vs. $\langle\Sigma_{gas}\rangle/t_{ff}$ in a different sample of clouds. We discuss possible differences in the two samples of star-forming clouds and the effects of stellar feedback on the relation between gas density and star formation rate.

357.6) Turbulence and Accretion: a High-resolution Study of the B5 Filaments
Michael Chun-Yuan Chen, James Di Francesco, Jaime E. Pineda, Stella S. Offner, Rachel K. Friesen

High-resolution observations of the Perseus B5 "core" have previously revealed that this subsonic region actually consists of several filaments that are likely in the process of forming a quadruple stellar system. Since subsonic filaments are thought to be produced at the $\sim$ 0.1 pc sonic scale by turbulent compression, a detailed kinematic study is crucial to test such a scenario in the context of core and star formation. Here we present a detailed kinematic follow-up study of the B5 filaments at a 0.009 pc resolution using the VLA and GBT combined observations fitted with multi-component spectral models. Using precisely identified filament spines, we find a remarkable resemblance between the averaged width profiles of each filament and Plummer-like functions, with filaments possessing FWHM widths of $\sim$ 0.03 pc. The velocity dispersion profiles of the filaments also show decreasing trends towards the filament spines. Moreover, the velocity gradient field in B5 appears to be locally well ordered ($\sim$ 0.04 pc) but globally complex, with kinematic behaviors suggestive of inhomogeneous turbulent accretion onto filaments and longitudinal flows towards a local overdensity along one of the filaments.

357.7) Rethinking the role of the giant planet instability in terrestrial planet formatic

Matthew S. Clement, Rogerio Deienno, Andre Izidoro

Advances in computing power and numerical methodologies over the past several decades sparked a prolific output of dynamical investigations of the late stages of terrestrial planet formation. Among other peculiar inner solar system qualities, the ability of simulations to reproduce the small mass of Mars within the planets' geochemically inferred accretion timescale of $\lesssim$10 Myr after the appearance of calcium aluminum-rich inclusions (CAIs) is arguably considered the gold standard for judging evolutionary hypotheses. At present, a number of independent models are capable of consistently generating Mars-like planets and simultaneously satisfying various important observational and geochemical constraints. However, all models must still account for the effects of the epoch of giant planet migration and orbital instability; an event which dynamical and cosmochemical constraints indicate occurred within the first 100 Myr after nebular gas dispersal. If the instability occurred in the first few Myr of this window, the disturbance might have affected the bulk of Mars' growth. In this manuscript, we turn our attention to a scenario where the instability took place after $t \simeq 50$ Myr. Specifically, we simulate the instability's effects on three nearly-assembled terrestrial systems that were generated via previous embryo accretion models and contain three large proto-planets (i.e. Earth, Venus and Theia) with $0.5 < m < 1.0\ M_\oplus$ and orbits interior to a collection of ~Mars-mass embryos (a >1.3 au and $m < 0.2\ M_\oplus$) and debris. While the instability consistently triggers a Moon-forming impact and efficiently removes excessive material from the Mars-region in our models, we find that our final systems are too dynamically excited and devoid of Mars and Mercury analogs. Thus, we conclude that, while possible, our scenario is far more improbable than one where the instability either occurred earlier, or at a time where Earth and Venus' orbits were far less dynamically excited than considered here.

357.9) A Population of Dipper Stars from the Transiting Exoplanet Survey Satellite Mission

Benjamin K. Capistrant, et al.

Dipper stars are a classification of young stellar objects that exhibit dimming variability in their light curves, dropping in brightness by 10-50%, likely induced by occultations due to circumstellar disk material. This variability can be periodic, quasi-periodic, or aperiodic. Dipper stars have been discovered in young stellar associations via ground-based and space-based photometric surveys. We present the detection and characterization of the largest collection of dipper stars to date: 293 dipper stars, including 234 new dipper candidates. We have produced a catalog of these targets, which also includes young stellar variables that exhibit predominately bursting-like variability and symmetric variability (equal parts bursting and dipping). The total number of catalog sources is 414. These variable sources were found in a visual survey of TESS light curves, where dipping-like variability was observed. We found a typical age among our dipper sources of <5 Myr, with the age distribution peaking at ≈ 2 Myr, and a tail of the distribution extending to ages older than 20 Myr. Regardless of the age, our dipper candidates tend to exhibit infrared excess, which is indicative of the presence of disks. TESS is now observing the ecliptic plane, which is rich in young stellar associations, so we anticipate many more discoveries in the TESS dataset. A larger sample of dipper stars would enhance the census statistics of light curve morphologies and dipper ages.